Research Square

Preprints are preliminary reports that have not undergone peer review.
They should not be considered conclusive, used to inform clinical practice,
or referenced by the media as validated information.

Selective detection of ^{13}CH signals from the mixture of $^{13}CH/^{13}CH_2/^{13}CH_3$ groups in biomolecules with enhanced sensitivity

Tairan Yuwen

tyuwen@stjude.org

St. Jude Children's Research Hospital

Zhilian Xia

St. Jude Children's Research Hospital

Jiangshu Liu

St. Jude Children's Research Hospital

Yixin Cui

St. Jude Children's Research Hospital

Jitendra Das

St. Jude Children's Research Hospital

Youlin Xia

St. Jude Children's Research Hospital

Paolo Rossi

St. Jude Children's Research Hospital

Charalampos G. Kalodimos

St. Jude Children's Research Hospital

Research Article

Keywords: Cross-polarization (CP), HSQC, INEPT, Preservation of equivalent pathways (PEP), Stereo-array isotope labeling (SAIL)

Posted Date: August 18th, 2026

DOI: https://doi.org/10.21203/rs.3.rs-10556147/v1

License: This work is licensed under a Creative Commons Attribution 4.0 International License.
Read Full License

Additional Declarations: No competing interests reported.

Abstract

The NMR spectra of ^{13}C-labeled biomolecules typically contain signals arising from ^{13}CH, $^{13}CH_2$, and $^{13}CH_3$ groups. In many applications, ^{13}CH group is of the primary interest since it exhibits relatively simple spin system and relaxation behavior. However, the selective detection of ^{13}CH signals in the presence of $^{13}CH_2$/$^{13}CH_3$ groups remains challenging, and many existing schemes are not well suited for biomolecular studies. In this work, we have developed an optimized pulse scheme, termed CH-selective $^{1}H–^{13}C$ HSQC, for selective detection of ^{13}CH signals from the mixtures containing ^{13}CH/$^{13}CH_2$/$^{13}CH_3$ groups. This method exploits one-bond $^{1}J_{CH}$ scalar coupling evolution to efficiently suppress signals from $^{13}CH_2$/$^{13}CH_3$ groups, while enhancing signal intensities of ^{13}CH resonances by exploiting cross-polarization (CP) based coherence transfer and preservation of equivalent pathways (PEP) methodology. This experiment offers distinct advantages over many other existing schemes developed for similar purposes, and is demonstrated using several protein samples. In addition, the experimental conditions to achieve optimal suppression of $^{13}CH_2$/$^{13}CH_3$ moieties are systematically investigated and discussed.

Introduction

Biomolecular samples with ^{13}C isotope labeling typically contain a mixture of ^{13}CH, $^{13}CH_2$, and $^{13}CH_3$ groups, corresponding to AX, AX_2, and AX_3 spin systems, respectively (Kay and Bull 1992). In two-dimensional $^{1}H–^{13}C$ correlation maps, signals from ^{13}CH/$^{13}CH_2$/$^{13}CH_3$ groups coexist, increasing the likelihood of resonance overlap and complicating further analysis, therefore it is desirable to selectively detect a specific spin system in many applications. Compared with the AX spin system, selective detection of AX_2 (Schmidt and Ruterjans 1990) or AX_3 (Kessler et al. 1991) spin system is relatively straightforward, since higher order coherences can be created in these spin systems which distinguish from the AX spin system. However, in many cases it is more desirable to selectively detect signals from ^{13}CH groups, since the spin system is relatively simple and the relaxation mechanism is more amenable to straightforward interpretation (Brath et al. 2006; Guo and Tugarinov 2010; Ishima et al. 1999; Ishima et al. 2001a; Ishima et al. 2001b; Kay and Bull 1992; Otten et al. 2010).

In our lab, $^{1}H–^{13}C$ methyl-labeled kinases have been widely used for structural determination and dynamics study (Cui et al. 2025; Xie et al. 2020). In methyl-labeled samples, the CH and CH_2 groups are replaced by ^{12}CD and $^{12}CD_2$ moieties, respectively, which substantially simplify the ^{1}H/^{13}C-related NMR spectra and reduce relaxation-induced signal decay. However, the deuteration of CH and CH_2 groups also decreases the proton density, resulting in a reduced network of nuclear Overhauser effect (NOE) contacts and consequently less structural information. To address this limitation, stereo-array isotope labeling (SAIL) residues can be introduced, where CH and CH_2 groups are replaced by ^{13}CH and ^{13}CHD moieties, respectively, thereby restoring strategically positioned protons while maintaining many of the favorable relaxation properties of deuteration (Kainosho et al. 2018; Kainosho et al. 2006). SAIL lysine

(Lys) or arginine (Arg) is most commonly used, since the long side chain provides a large number of NOE contacts, and one of the lysine residues is located in the kinase binding pocket, making it particularly useful for probing the local binding environment. As a result, kinase samples prepared with both methyl labeling and SAIL lysine contain signals from both ^{13}CH and $^{13}CH_3$ groups in $^{1}H–^{13}C$ HSQC spectra. Selective detection of the ^{13}CH resonances is therefore desirable for simplifying spectral analysis and facilitating resonance assignment.

In principle, the selective detection of ^{13}CH groups can be achieved by exploiting the different responses of AX, AX_2, and AX_3 spin systems to one-bond $^{1}J_{CH}$ scalar coupling evolution. However, many existing schemes are designed for studying small molecules, which are not fully optimized in terms of intrinsic sensitivity. For example, DEPT-90 suffers from low signal-to-noise due to ^{13}C direct detection (Doddrell et al. 1982), whereas inverse DEPT initiates magnetization transfer from ^{13}C instead of ^{1}H (Bendall et al. 1983). Several other approaches, such as HYSEL (Stelten and Leibfritz 1996), MAXY (Liu et al. 1995), and HmQC (Parella et al. 1995), generate multiple-quantum coherences and apply coherence-selection gradients to select signals from a specific spin system. However, these approaches suffer from sensitivity losses since only a specific coherence transfer pathway is preserved. In addition, heteronuclear single quantum correlation (HSQC)-based experiments are generally preferred over heteronuclear multiple quantum correlation (HMQC)-based methods for biomolecular applications targeting AX spin systems, as the HSQC-based scheme is less affected by $^{1}H–^{1}H$ dipolar interactions, leading to improved spectral resolution and sensitivity (Bax et al. 1990; Norwood et al. 1990).

Among several $^{1}H–^{13}C$ HSQC-based approaches for selective detection of ^{13}CH signals, most schemes are not ideally suited for biomolecular studies. For example, although DEPT-HSQC can distinguish ^{13}CH from $^{13}CH_2/^{13}CH_3$ groups through opposite signs, it cannot eliminate $^{13}CH_2/^{13}CH_3$ signals completely (Tate et al. 1991). Likewise, gradient-enhanced multiplicity-edited HSQC exhibits imperfect spin system selectivity, often leaving substantial residual $^{13}CH_3$ signals (Parella et al. 1997). In general, the major issue in ^{13}CH-selective experiments arises from the suppression of $^{13}CH_3$ signals, as these signals are intrinsically strong due to large number of ^{1}H spins and the favorable relaxation property associated with rapid methyl group rotation (Tugarinov et al. 2003). Moreover, $^{13}CH_3$ and ^{13}CH groups have the same parity with respect to the number of attached ^{1}H spins, making their discrimination based on $^{1}J_{CH}$ scalar coupling evolution particularly difficult. For the purpose of suppressing $^{13}CH_3$ signals, purging elements have been introduced to dephase the magnetization from $^{13}CH_3$ groups (Brath et al. 2006; Ishima et al. 1999; Mittermaier and Kay 2002). However, this strategy is only partially effective even for small proteins due to differential relaxation among various multiplet components (Brath et al. 2006; Mittermaier and Kay 2002). For larger biomolecules, where cross-correlated relaxation effects are more pronounced, such purging scheme provides only marginal reduction to $^{13}CH_3$ signal intensity.

In this work, we have developed an optimized $^{1}H–^{13}C$ HSQC pulse scheme for selective detection of ^{13}CH signals from the mixture of $^{13}CH/^{13}CH_2/^{13}CH_3$ groups. Compared with other existing approaches, the new scheme provides more efficient suppression of $^{13}CH_2/^{13}CH_3$ moieties while preserving ^{13}CH signal intensity. In addition, this experiment is compatible with a broad range of applications targeting ^{13}CH groups, such as structural (Kay et al. 1993) and dynamics (Hansen et al. 2013; Hansen et al. 2008; Lundström and Akke 2005; Weininger et al. 2013; Yamazaki et al. 1994) studies of biomolecules.

Material and Methods

Sample preparation

A total of six samples were used in this study. Three samples of [U-^{2}H; Ileδ1-$^{13}CH_3$; Leu,Val-$^{13}CH_3/^{13}CH_3$; Met-$^{13}CH_3$]-labeled, [U-^{2}H; Ileδ1-$^{13}CHD_2$; Leu,Val-$^{13}CHD_2/^{13}CHD_2$; Met-$^{13}CHD_2$]-labeled, and [U-^{13}C]-labeled B1 domain of peptostreptococcal protein L (denoted as protein L hereafter), respectively, were prepared in accordance with the established protocols (Mittermaier and Kay 2001). The samples were in a 95% H_2O/5% D_2O buffer (pH 6.0) containing 50 mM sodium phosphate, 0.05% NaN_3, with ~ 2 mM concentration for each sample. These three samples are referred to as ILVM-$^{13}CH_3$-labeled protein L, ILVM-$^{13}CHD_2$-labeled protein L, and [U-^{13}C]-labeled protein L, respectively. Two samples of [U-^{2}H; Ileδ1-$^{13}CH_3$; Leu,Val-$^{13}CH_3/^{13}CH_3$; Met-$^{13}CH_3$]-labeled, and [U-^{2}H; Ileδ1-$^{13}CHD_2$; Leu,Val-$^{13}CHD_2/^{13}CHD_2$; Met-$^{13}CHD_2$]-labeled L99A T4 lysozyme samples (designated as L99A T4L henceforth), respectively, were generated according to Bouvignies et al. (Bouvignies et al. 2011), in a 95% H_2O/5% D_2O buffer (pH 5.5) containing 50 mM sodium phosphate, 25 mM NaCl, 2 mM EDTA, 0.05% NaN_3, and the concentration of each sample was ~ 2 mM. These two samples are referred to as ILVM-$^{13}CH_3$-labeled L99A T4L, and ILVM-$^{13}CHD_2$-labeled L99A T4L, respectively. The last sample, [U-^{2}H; Ileδ1-$^{13}CH_3$; Leu,Val-$^{13}CH_3/^{13}CH_3$; Met-$^{13}CH_3$; Ala-$^{13}CH_3$; Thr-$^{13}CH_3$; SAIL-Lys]-labeled V600E BRAF (Residues 448–723), denoted as ILVMAT-$^{13}CH_3$ + SAIL-Lys labeled BRAF hereafter, was prepared as described previously (Grasso et al. 2016), with ~ 400 µM protein dissolved in a 95% H_2O/5% D_2O buffer (pH 7.5) containing 25 mM sodium phosphate, 50 mM NaCl, 1 mM EDTA, and 2.5 mM BME.

NMR spectroscopy

NMR experiments were conducted on Bruker 800 MHz spectrometer equipped with *z*-axis gradient cryogenically cooled TCI probe. All experiments were performed at 25°C except for ILVMAT-$^{13}CH_3$ + SAIL-Lys labeled BRAF, which were performed at 10°C. A pre-scan delay of 1.0 s, acquisition time of 100 ms and the number of transients of 4 were utilized for collecting all data sets. The ^{13}C carrier was set to ~ 35 ppm for [U-^{13}C]-labeled protein-L and ILVMAT-$^{13}CH_3$ + SAIL-Lys labeled BRAF, and to ~ 15 ppm for all other samples. The radiofrequency (RF) field strength used for cross-polarization (CP) was ~ 15 kHz

for [U-^{13}C]-labeled protein L and ILVMAT-$^{13}CH_3$ + SAIL-Lys labeled BRAF, and ~ 10 kHz for other samples. Regular ^{1}H–^{13}C HSQC and CH-selective ^{1}H–^{13}C HSQC were carried out for each sample. The multiplicity-edited variant of regular ^{1}H–^{13}C HSQC (Davis 1991) were recorded for [U-^{13}C]-labeled protein L and ILVMAT-$^{13}CH_3$ + SAIL-Lys labeled BRAF, which yield opposite signs for signals from ^{13}CH/$^{13}CH_3$ groups and from $^{13}CH_2$ groups.

Data analysis

All NMR datasets were processed and analyzed using the *NMRPipe* suite of programs (Delaglio et al. 1995), and peak intensities were extracted using the *autoFit* subroutine. Each spectrum was scaled to yield the same noise level for the comparison of relative signal intensity. Statistical analysis was performed based on all peaks in the spectra, and the intensity was reported as the ratio relative to the corresponding intensity in regular ^{1}H–^{13}C HSQC (without multiplicity editing).

Numerical simulation

All numerical simulations were carried out using home-written Python programs. The evolution of the spin density matrix (ρ) was computed using the Liouville–von Neumann equation (Allard et al. 1998). The forward magnetization transfer from ^{1}H to ^{13}C was simulated with insensitive nuclei enhanced by polarization transfer (INEPT) or CP-based coherence transfer scheme. For INEPT-based coherence transfer scheme, the initial density matrix corresponds to $2C_zH_z$ magnetization, whereas for CP-based coherence transfer scheme, the initial density matrix corresponds to H_z magnetization. In this work, H_z represents $\sum_i \mathrm{H}_z^i$, $2C_zH_z$ represents $\sum_i 2\mathrm{C}_z\mathrm{H}_z^i$, and $4C_zH_zH_z$ represents $\sum_{i,j} 4\mathrm{C}_z\mathrm{H}_z^i\mathrm{H}_z^j$ for $^{13}CH_2$ groups (i,j = 1,2; $i \neq j$) or $^{13}CH_3$ groups (i,j = 1,2,3; $i \neq j$), in order to take the permutation of multiple ^{1}H spins into account.

Results and Discussion

Suppression of signals from $^{13}CH_2$/$^{13}CH_3$ groups in CH-selective ^{1}H–^{13}C HSQC

In regular ^{1}H–^{13}C HSQC, signals from $^{13}CH_2$/$^{13}CH_3$ groups increase spectral crowding and cause overlap with ^{13}CH resonances, which potentially complicate further analyses based on ^{13}CH groups. In order to selectively detect ^{13}CH signals from the mixture of ^{13}CH/$^{13}CH_2$/$^{13}CH_3$ groups, refocused INEPT is commonly used to discriminate different spin systems based on one-bond $^{1}J_{CH}$ scalar coupling evolution. The pulse scheme of CH-selective ^{1}H–^{13}C HSQC experiment is shown in Fig. 1, which is optimized based on the work of Tugarinov et al. to selectively detect $^{13}CHD_2$ methyl isotopomers from

the mixture of $^{13}CH_3/^{13}CH_2D/^{13}CHD_2$ species (Liao and Tugarinov 2011). In this experiment, the delay time τ_c is set to ~ $1/(4^1J_{CH})$, such that the single-spin or multiple-spin orders present at point "B" of Fig. 1 that are converted into observables correspond to C_z (for ^{13}CH groups), $2C_zH_z$ (for $^{13}CH_2$ groups), or $4C_zH_zH_z$ (for $^{13}CH_3$ groups). The delay time τ_b is adjusted to achieve optimal suppression of $^{13}CH_2/^{13}CH_3$ signals. In the absence of relaxation effects, $\tau_b = 1/(4^1J_{CH})$ is optimal for suppressing $^{13}CH_2$ signals, since the magnitudes of spin orders C_z, $2C_zH_z$, and $4C_zH_zH_z$ are all close to zero (Fig. S1), leading to cleaner suppression of $^{13}CH_2$ signals, as the spin orders C_z and $4C_zH_zH_z$ can still be converted into observables in the case that τ_c is not exact $1/(4^1J_{CH})$ due to variations of $^1J_{CH}$ among multiple $^{13}CH_2$ groups. In contrast, optimal suppression of $^{13}CH_3$ signals requires a shorter delay, with $\tau_b \simeq 0.608/(4^1J_{CH})$, which makes the amplitude of the spin order $4C_zH_zH_z$ close to zero (Liao and Tugarinov 2011). The optimal experimental setup for studying different types of samples is summarized in Table 1. When relaxation effects are present, the optimal τ_b for suppressing $^{13}CH_3$ signals becomes even shorter for larger biomolecules due to cross-correlated relaxation effects (Tables 2, 3), therefore the value of τ_b should be optimized experimentally (Figs. S2, S3) (Liao and Tugarinov 2011). Since CH-selective $^1H–^{13}C$ HSQC creates ^{13}C in-phase magnetization, this scheme is compatible with a range of downstream applications, such as the structural (Kay et al. 1993) and dynamics (Weininger et al. 2013; Yamazaki et al. 1994) studies of biomolecules based on ^{13}C or ^1H spins in ^{13}CH groups.

Table 1

Optimal experimental setup for studying different types of samples with CH-selective $^1H–^{13}C$ HSQC

Suppressed groups	**τ_b (INEPT)**	**τ_{mix} (CP)**	**τ_c**	**Signal intensity of ^{13}CH group**
$^{13}CH_2$ only	$1/(4^1J_{CH2})$	$\sqrt{2}/^1J_{CH2}$	$1/(4^1J_{CH2})$	1.0 (INEPT) or 0.633 (CP)
$^{13}CH_3$ only	~ $0.608/(4^1J_{CH3})$ (need to optimize)	~ $0.818/^1J_{CH3}$ (need to optimize)	$1/(4^1J_{CH1})$	0.816 (INEPT) or 0.921 (CP)
$^{13}CH_2$ and $^{13}CH_3$	~ $0.608/(4^1J_{CH3})$ (need to optimize)	~ $0.818/^1J_{CH3}$ (need to optimize)	$1/(4^1J_{CH2})$	0.816 (INEPT) or 0.921 (CP)

Note: $^1J_{CH1}/^1J_{CH2}/^1J_{CH3}$ represents one-bond $^1H–^{13}C$ scalar coupling of $^{13}CH/^{13}CH_2/^{13}CH_3$ moieties. The value of $\tau_a = 1/(4^1J_{CH1})$ is used in each case. The signal intensity of ^{13}CH group is calculated as the ratio relative to regular $^1H–^{13}C$ HSQC with the assumption of $^1J_{CH1} = {}^1J_{CH2} = {}^1J_{CH3}$ and without relaxation effects.

The ^1H spin-lock purge pulses (Messerle et al. 1989) are applied before the ^{13}C frequency labeling period, which not only help to improve water suppression but also attenuate residual signals from

$^{13}CH_2/^{13}CH_3$ groups. Compared with the experiment performed without ^1H spin-lock purge pulses, the residual signals of $^{13}CH_2/^{13}CH_3$ groups are reduced by up to 50%. At the same time, it causes minimal loss to ^{13}CH signals, since ^{13}C magnetization is aligned along *z*-axis during the application of ^1H spin-lock purge pulses.

Improvement of signal intensity from CH groups in CH-selective H–C HSQC

Several additional modifications are introduced in CH-selective $^1H–^{13}C$ HSQC experiment to improve signal intensities of ^{13}CH groups. In particular, the forward magnetization transfer from ^1H to ^{13}C can be implemented with cross-polarization (CP) (Ernst et al. 1991) instead of refocused INEPT. In CP-based coherence transfer scheme, a mixing time (τ_{mix}) of ~ $0.818/^1J_{CH}$ minimizes the magnitude of spin order $4C_zH_zH_z$ generated for $^{13}CH_3$ groups in the absence of relaxation (Fig. 2), which creates higher ^{13}CH signal intensity than INEPT-based scheme under the condition optimized for $^{13}CH_3$ suppression (Table 1). Similar to the case of INEPT-based scheme, relaxation effects shorten the optimal τ_{mix} value, especially for biomolecules with longer rotational correlation times (Tables 2, 3). Therefore, the optimal τ_{mix} should be determined for each sample experimentally, typically using one-dimensional version of CH-selective $^1H–^{13}C$ HSQC (Figs. S2, S3).

The CP-based coherence transfer scheme is particularly advantageous for studying biomolecules with μs–ms timescale dynamics, which are usually functionally relevant (Jin et al. 2025). Such slow exchange processes increase the effective transverse relaxation rates, $R_{2,eff}$, leading to additional signal loss during coherence transfer steps (Jin et al. 2025). In CP-based coherence transfer scheme, high-power RF fields (≥ 10 kHz) are applied on both ^1H and ^{13}C channels simultaneously, thereby largely suppressing exchange-induced $R_{2,eff}$ during coherence transfer steps (Levitt 1991). For several residues in L99A T4L involved in μs–ms timescale exchange process (e.g. M102 and M106) (Bouvignies et al. 2011), signal enhancement up to 50% was observed with CP-based coherence transfer scheme.

Despite these advantages, CP-based scheme also has certain limitations. Since high-power RF fields (≥ 10 kHz) are applied on both channels, CP-based scheme suffers from higher duty cycle than INEPT-based scheme, which may induce greater sample heating effects. In addition, when the system under investigation spans a broad range of ^1H and ^{13}C resonance offsets, as is often the case at higher magnetic fields, the coherence transfer efficiency of CP-based scheme is deteriorated due to large off-resonance effects (Levitt 1991), and the optimal τ_{mix} varies with the RF field strength, whereas INEPT-based scheme is less affected by such issues. Furthermore, when only $^{13}CH_2$ signals need to be suppressed, the INEPT-based scheme is generally preferred, since it generates higher ^{13}CH signal intensity than CP-based scheme under the condition optimized for $^{13}CH_2$ suppression (Table 1).

Another improvement in ^{13}CH signal intensity arises from the implementation of preservation of equivalent pathways (PEP) methodology (Palmer et al. 1991), which is commonly used in sensitivity-enhanced HSQC experiments (Fig. 3). For AX spin system, the sensitivity-enhanced scheme provides an intrinsic signal-to-noise improvement of √2 relative to the unenhanced scheme in the absence of relaxation, although the actual sensitivity gain is always less than the theoretical √2 factor due to longer pulse sequence duration and relaxation effects (Palmer et al. 1991). In addition, the sensitivity-enhanced implementation can be combined with coherence-selection gradients, improving artifact suppression without decreasing intrinsic sensitivity (Dotsch et al. 1995). For AX_2 and AX_3 spin systems, only 50% of the magnetization is converted into observables, therefore signals from AX_2/AX_3 groups are expected to be better attenuated with the sensitivity-enhanced implementation. In general, the sensitivity-enhanced scheme is more advantageous for small molecules or mobile groups (such as $^{13}CHD_2$-labeled methyl groups), whereas the unenhanced scheme is preferable for large biomolecules, for which relaxation losses during coherence transfer steps become more pronounced (Palmer et al. 1991). The optimal implementation (INEPT-based vs. CP-based, unenhanced vs. sensitivity-enhanced) for investigating each specific biomolecule can be determined based on ^{13}CH signal intensities in one-dimensional version of the experiment. For ILVM-$^{13}CHD_2$-labeled protein L and L99A T4L, the CP-based, sensitivity-enhanced scheme shows higher ^{13}CH signal intensity than other schemes (Tables 2, 3). It should be noted that τ_b or τ_{mix} for optimal suppression of $^{13}CH_2$/$^{13}CH_3$ moieties is usually slightly shorter in the sensitivity-enhanced scheme than the unenhanced scheme, therefore should be optimized separately for each implementation (Tables 2–5).

Table 2

Summary of the results obtained with different schemes of CH-selective ^{1}H–^{13}C HSQC for ILVM-$^{13}CH_3$- and ILVM-$^{13}CHD_2$-labeled protein L

Scheme	τ_b (INEPT)	τ_{mix} (CP)	τ_c	$^{13}CH_3$ group intensity	^{13}CH group intensity
INEPT, unenhanced	1.15 ms	–	2.0 ms	0.03 ± 0.02	0.78 ± 0.02
CP, unenhanced	–	6.3 ms		0.03 ± 0.02	0.86 ± 0.02
INEPT, enhanced	1.14 ms	–		0.03 ± 0.02	0.99 ± 0.02
CP, enhanced	–	6.2 ms		0.03 ± 0.02	1.11 ± 0.03

Note: The average value of $^1J_{CH}$ for ^{13}CH/$^{13}CH_3$ moieties in ILVM-$^{13}CHD_2$- and ILVM-$^{13}CH_3$-labeled protein L was 125 Hz according to coupled ^{1}H–^{13}C HSQC (based on Ile/Leu/Val). The optimal τ_b or τ_{mix} was determined based on the ILVM-$^{13}CH_3$-labeled sample, which was also used for measuring the ILVM-$^{13}CHD_2$-labeled sample. The intensities of ^{13}CH/$^{13}CH_3$ groups are reported as the ratio relative to the corresponding intensity in regular ^{1}H–^{13}C HSQC. The mean value and standard deviation of the ratios were obtained based on all peaks in the spectra.

Table 3

Summary of the results obtained with different schemes of CH-selective $^{1}H–^{13}C$ HSQC for ILVM-$^{13}CH_3$- and ILVM-$^{13}CHD_2$-labeled L99A T4L

Scheme	τ_b (INEPT)	τ_{mix} (CP)	τ_c	$^{13}CH_3$ group intensity	^{13}CH group intensity
INEPT, unenhanced	1.09 ms	–	2.0 ms	0.05 ± 0.03	0.73 ± 0.04
CP, unenhanced	–	6.0 ms		0.05 ± 0.04	0.82 ± 0.06
INEPT, enhanced	1.08 ms	–		0.06 ± 0.04	0.91 ± 0.06
CP, enhanced	–	5.9 ms		0.06 ± 0.04	1.02 ± 0.05

Application of CH-selective H–C HSQC for studying biomolecules

The CH-selective $^{1}H–^{13}C$ HSQC experiment was carried out for two additional protein samples. For [U-^{13}C]-labeled protein L, signals from $^{13}CH_2/^{13}CH_3$ groups are more intense than ^{13}CH groups in regular $^{1}H–^{13}C$ HSQC, which could potentially interfere with the structural or dynamics study based on $^{13}C^{\alpha}$ sites (Fig. 4A) (Hansen et al. 2013; Hansen et al. 2008; Lundström and Akke 2005; Yamazaki et al. 1994). In contrast, most $^{13}CH_2/^{13}CH_3$ signals are suppressed to a satisfactory level, and those ^{13}CH resonances overlapped with $^{13}CH_2/^{13}CH_3$ peaks in regular $^{1}H–^{13}C$ HSQC can be clearly identified in CH-selective $^{1}H–^{13}C$ HSQC (Fig. 4B). Due to relatively small molecular weight of protein L (~ 7 kDa), the sensitivity-enhanced implementation shows higher intensities than the unenhanced scheme for most residues, and CP-based scheme exhibits higher overall sensitivity than INEPT-based scheme (Table 4).

Table 4

Summary of the results obtained with different schemes of CH-selective $^{1}H–^{13}C$ HSQC for [U-^{13}C]-labeled protein L

Scheme	**τ_b (INEPT)**	**τ_{mix} (CP)**	**τ_c**	**$^{13}CH_2/^{13}CH_3$ group intensity**	**^{13}CH group intensity**
INEPT, unenhanced	1.13 ms	–	1.85 ms	0.04 ± 0.03	0.66 ± 0.04
CP, unenhanced	–	6.5 ms		0.04 ± 0.03	0.71 ± 0.08
INEPT, enhanced	1.13 ms	–		0.03 ± 0.02	0.72 ± 0.08
CP, enhanced	–	6.3 ms		0.03 ± 0.02	0.79 ± 0.10

Note: The average values of $^{1}J_{CH}$ for $^{13}CH/^{13}CH_2/^{13}CH_3$ moieties in [U-^{13}C]-labeled protein L were 140/135/125 Hz according to coupled $^{1}H–^{13}C$ HSQC (based on Ile/Leu/Val for $^{13}CH_3$ groups). The intensity of $^{13}CH/^{13}CH_2/^{13}CH_3$ group is reported as the ratio relative to the corresponding intensity in regular $^{1}H–^{13}C$ HSQC (without multiplicity editing). The mean value and standard deviation of the ratios were obtained based on all peaks in the spectra.

The CH-selective $^{1}H–^{13}C$ HSQC scheme was also demonstrated using ILVMAT-$^{13}CH_3$ + SAIL-Lys labeled BRAF, which is a kinase within the mitogen-activated protein kinase (MAPK) signaling pathway. In regular $^{1}H–^{13}C$ HSQC, the strong $^{13}CH_3$ signals obscure the identification of the nearby weak ^{13}CH signals from SAIL-Lys, which preclude the extraction of structural information from these sites (Fig. 5A). In contrast, in CH-selective $^{1}H–^{13}C$ HSQC, residual $^{13}CH_3$ signals are attenuated substantially, allowing those signals from SAIL-Lys to be identified more clearly (Fig. 5B). Because of the relatively high molecular weight of BRAF (~ 30 kDa), ^{13}CH signal intensities in the sensitivity-enhanced implementation are comparable to the unenhanced scheme, while the CP-based scheme still offers higher sensitivity than the INEPT-based scheme (Table 5). In general, it is difficult to completely suppress $^{13}CH_3$ signals for high-molecular-weight biomolecules due to site-dependent variations of $^{1}J_{CH}$ scalar coupling constants and relaxation properties (Liao and Tugarinov 2011). Nevertheless, the CH-selective $^{1}H–^{13}C$ HSQC can still achieve satisfactory suppression of $^{13}CH_2/^{13}CH_3$ moieties for large biomolecules with careful experimental setup.

Table 5

Summary of the results obtained with different schemes of CH-selective $^{1}H–^{13}C$ HSQC for ILVMAT-$^{13}CH_3$ + SAIL-Lys labeled BRAF

Scheme	τ_b (INEPT)	τ_{mix} (CP)	τ_c	$^{13}CH_2/^{13}CH_3$ group intensity	^{13}CH group intensity
INEPT, unenhanced	0.88 ms	–	1.85 ms	0.06 ± 0.04	0.45 ± 0.11
CP, unenhanced	–	5.1 ms		0.05 ± 0.04	0.48 ± 0.13
INEPT, enhanced	0.89 ms	–		0.08 ± 0.05	0.45 ± 0.14
CP, enhanced	–	5.0 ms		0.07 ± 0.05	0.50 ± 0.16

Conclusions

In this work, we have developed an optimized pulse scheme, termed CH-selective $^{1}H–^{13}C$ HSQC, for selective detection of ^{13}CH signals from the mixture of $^{13}CH/^{13}CH_2/^{13}CH_3$ groups. This experiment provides efficient suppression of $^{13}CH_2/^{13}CH_3$ moieties while preserving ^{13}CH signal intensities by exploiting CP-based coherence transfer and PEP methodology, making it better suited for biomolecular studies than most other existing approaches. Since this scheme is designed for selectively detecting AX spin system from the mixture of $AX/AX_2/AX_3$ spin systems, it can be readily adapted for the measurement of other groups (such as $^{15}NH/^{15}NH_2$), where analogous spin system selection is desirable. In addition, this experiment is also compatible with many other downstream applications targeting ^{13}CH groups, such as the investigation of structural and dynamic properties of biomolecules.

Declarations

Supplementary Information

The Supplementary Information includes supplementary figures, and the pulse sequence code for Bruker spectrometers.

Author Contribution

T.Y. and C.G.K conceptualized the work. X.Z., J.L., Y.C., and J.D. prepared the protein samples. T.Y. performed the NMR experiments, analyzed the data, and prepared all the figures. T.Y., Y.X., P.R. and C.G.K. wrote the manuscript. All authors reviewed the manuscript.

Acknowledgement

This work was conducted within the framework of the Blue Sky Initiative “Seeing the Invisible in Protein Kinases” at St. Jude Children’s Research Hospital. This work is financially supported by USA NIH Grant R35 GM122462 to C.G.K., by the National Natural Science Foundation of China (NSFC) Grant 22474006 to T.Y., and by the Biomolecular NMR Center, St. Jude Children’s Research Hospital. We thank Dr. Jinsong Fan and Dr. Mary Clay for insightful discussions.

Data Availability

The pulse programs and parameter sets are available on GitHub at https://github.com/tyuwen/chsqc_G5.

References

1. Allard P, Helgstrand M, Härd T (1998) The complete homogeneous master equation for a heteronuclear two-spin system in the basis of Cartesian product operators. J Magn Reson 134:7-16. https://doi.org/10.1006/jmre.1998.1509
2. Bax A, Ikura M, Kay LE, Torchia DA, Tschudin R (1990) Comparison of different modes of two-dimensional reverse-correlation NMR for the study of proteins. J Magn Reson 86:304-318. https://doi.org/10.1016/0022-2364(90)90262-8
3. Bendall MR, Pegg DT, Doddrell DM, Field J (1983) Inverse DEPT sequence. Polarization transfer from a spin-1/2 nucleus to *n* spin-1/2 heteronuclei via correlated motion in the doubly rotating reference frame. J Magn Reson 51:520-526. https://doi.org/10.1016/0022-2364(83)90303-7
4. Bouvignies G, Vallurupalli P, Hansen DF, Correia BE, Lange O, Bah A, Vernon RM, Dahlquist FW, Baker D, Kay LE (2011) Solution structure of a minor and transiently formed state of a T4 lysozyme mutant. Nature 477:111-114. https://doi.org/10.1038/nature10349
5. Brath U, Akke M, Yang D, Kay LE, Mulder FAA (2006) Functional dynamics of human FKBP12 revealed by methyl ^{13}C rotating frame relaxation dispersion NMR spectroscopy. J Am Chem Soc 128:5718-5727. https://doi.org/10.1021/ja0570279
6. Cui Y, Ali R, Clay M, Rossi P, Liu A, Yang D, Gough NR, Geiger T, Kalodimos CG (2025) Conformational landscape adaptations enable processive phosphorylation by Src family kinases. Science 390:eadw8310. https://doi.org/10.1126/science.adw8310
7. Davis DG (1991) Improved multiplet editing of proton-detected, heteronuclear shift-correlation spectra. J Magn Reson 91:665-672. https://doi.org/10.1016/0022-2364(91)90398-D
8. Delaglio F, Grzesiek S, Vuister GW, Zhu G, Pfeifer J, Bax A (1995) NMRPipe: A multidimensional spectral processing system based on UNIX pipes. J Biomol NMR 6:277-293. https://doi.org/10.1007/Bf00197809
9. Doddrell DM, Pegg DT, Bendall MR (1982) Distortionless enhancement of NMR signals by polarization transfer. J Magn Reson 48:323-327. https://doi.org/10.1016/0022-2364(82)90286-4

10. Dotsch V, Oswald RE, Wagner G (1995) Water suppression by coherence selection with absorptive lineshape without loss in sensitivity. J Magn Reson 108:285-288. https://doi.org/10.1006/jmrb.1995.1135
11. Ernst M, Griesinger C, Ernst RR, Bermel W (1991) Optimized heteronuclear cross polarization in liquids. Mol Phys 74:219-252. https://doi.org/10.1080/00268979100102191
12. Grasso M, Estrada MA, Ventocilla C, Samanta M, Maksimoska J, Villanueva J, Winkler JD, Marmorstein R (2016) Chemically linked vemurafenib inhibitors promote an inactive $BRAF^{V600E}$ conformation. ACS Chem Biol 11:2876-2888. https://doi.org/10.1021/acschembio.6b00529
13. Guo C, Tugarinov V (2010) Selective $^{1}H–^{13}C$ NMR spectroscopy of methyl groups in residually protonated samples of large proteins. J Biomol NMR 46:127-133. https://doi.org/10.1007/s10858-009-9393-0
14. Hansen AL, Bouvignies G, Kay LE (2013) Probing slowly exchanging protein systems via $^{13}C^{\alpha}$-CEST: Monitoring folding of the Im7 protein. J Biomol NMR 55:279-289. https://doi.org/10.1007/s10858-013-9711-4
15. Hansen DF, Vallurupalli P, Lundström P, Neudecker P, Kay LE (2008) Probing chemical shifts of invisible states of proteins with relaxation dispersion NMR spectroscopy: How well can we do? J Am Chem Soc 130:2667-2675. https://doi.org/10.1021/ja078337p
16. Ishima R, Louis JM, Torchia DA (1999) Transverse ^{13}C relaxation of CHD_2 methyl isotopmers to detect slow conformational changes of protein side chains. J Am Chem Soc 121:11589-11590. https://doi.org/10.1021/ja992836b
17. Ishima R, Louis JM, Torchia DA (2001a) Characterization of two hydrophobic methyl clusters in HIV-1 protease by NMR spin relaxation in solution. J Mol Biol 305:515-521. https://doi.org/10.1006/jmbi.2000.4321
18. Ishima R, Petkova AP, Louis JM, Torchia DA (2001b) Comparison of methyl rotation axis order parameters derived from model-free analyses of ^{2}H and ^{13}C longitudinal and transverse relaxation rates measured in the same protein sample. J Am Chem Soc 123:6164-6171. https://doi.org/10.1021/ja0104711
19. Jin Y, Cui Y, Yuwen T (2025) NMR methods for investigating functionally relevant biomolecular dynamics. Magn Reson Lett 5:200195. https://doi.org/10.1016/j.mrl.2025.200195
20. Kainosho M, Miyanoiri Y, Terauchi T, Takeda M (2018) Perspective: next generation isotope-aided methods for protein NMR spectroscopy. J Biomol NMR 71:119-127. https://doi.org/10.1007/s10858-018-0198-x
21. Kainosho M, Torizawa T, Iwashita Y, Terauchi T, Ono AM, Güntert P (2006) Optimal isotope labelling for NMR protein structure determinations. Nature 440:52-57. https://doi.org/10.1038/nature04525
22. Kay LE, Bull TE (1992) Heteronuclear transverse relaxation in AMX, AX_2, and AX_3 spin systems. J Magn Reson 99:615-622. https://doi.org/10.1016/0022-2364(92)90218-V

23. Kay LE, Keifer P, Saarinen T (1992) Pure absorption gradient enhanced heteronuclear single quantum correlation spectroscopy with improved sensitivity. J Am Chem Soc 114:10663-10665. https://doi.org/10.1021/ja00052a088
24. Kay LE, Xu G, Singer AU, Muhandiram DR, Forman-Kay JD (1993) A gradient-enhanced HCCH-TOCSY experiment for recording side-chain ^{1}H and ^{13}C correlations in H_2O samples of proteins. J Magn Reson 101:333-337. https://doi.org/10.1006/jmrb.1993.1053
25. Kessler H, Schmieder P, Kock M, Reggelin M (1991) Selection of methyl resonances in proton-detected heteronuclear shift correlation, the HQQC experiment. J Magn Reson 91:375-379. https://doi.org/10.1016/0022-2364(91)90199-4
26. Levitt MH (1991) Heteronuclear cross polarization in liquid-state nuclear magnetic resonance: Mismatch compensation and relaxation behavior. J Chem Phys 94:30-38. https://doi.org/10.1063/1.460398
27. Liao X, Tugarinov V (2011) Selective detection of $^{13}CHD_2$ signals from a mixture of $^{13}CH_3/^{13}CH_2D/^{13}CHD_2$ methyl isotopomers in proteins. J Magn Reson 209:101-107. https://doi.org/10.1016/j.jmr.2010.12.014
28. Liu M, Farrant RD, Nicholson JK, Lindon JC (1995) Selective detection of ^{1}H NMR resonances of CH_n groups using a heteronuclear maximum-quantum filter and pulsed field gradients. J Magn Reson 106:270-278. https://doi.org/10.1006/jmrb.1995.1043
29. Lundström P, Akke M (2005) Microsecond protein dynamics measured by $^{13}C^{\alpha}$ rotating-frame spin relaxation. ChemBioChem 6:1685-1692. https://doi.org/10.1002/cbic.200500086
30. Manu VS, Veglia G (2015) Genetic algorithm optimized triply compensated pulses in NMR spectroscopy. J Magn Reson 260:136-143. https://doi.org/10.1016/j.jmr.2015.09.010
31. Marion D, Ikura M, Tschudin R, Bax A (1989) Rapid recording of 2D NMR spectra without phase cycling. Application to the study of hydrogen exchange in proteins. J Magn Reson 85:393-399. https://doi.org/10.1016/0022-2364(89)90152-2
32. Messerle BA, Wider G, Otting G, Weber C, Wuthrich K (1989) Solvent suppression using a spin lock in 2D and 3D NMR spectroscopy with H_2O solutions. J Magn Reson 85:608-613. https://doi.org/10.1016/0022-2364(89)90252-7
33. Mittermaier A, Kay LE (2001) χ_1 torsion angle dynamics in proteins from dipolar couplings. J Am Chem Soc 123:6892-6903. https://doi.org/10.1021/ja010595d
34. Mittermaier A, Kay LE (2002) Effect of deuteration on some structural parameters of methyl groups in proteins as evaluated by residual dipolar couplings. J Biomol NMR 23:35-45. https://doi.org/Doi 10.1023/A:1015368803552
35. Norwood TJ, Boyd J, Heritage JE, Soffe N, Campbell ID (1990) Comparison of techniques for ^{1}H-detected heteronuclear $^{1}H–^{15}N$ spectroscopy. J Magn Reson 87:488-501. https://doi.org/10.1016/0022-2364(90)90306-T

36. Otten R, Chu B, Krewulak KD, Vogel HJ, Mulder FAA (2010) Comprehensive and cost-effective NMR spectroscopy of methyl groups in large proteins. J Am Chem Soc 132:2952-2960. https://doi.org/10.1021/ja907706a
37. Palmer AG, Cavanagh J, Wright PE, Rance M (1991) Sensitivity improvement in proton-detected two-dimensional heteronuclear correlation NMR spectroscopy. J Magn Reson 93:151-170. https://doi.org/10.1016/0022-2364(91)90036-S
38. Parella T, Sánchez-Ferrando F, Virgili A (1995) Clean proton editing using a gradient-selected multiple-quantum filter. J Magn Reson Ser A 117:78-83. https://doi.org/10.1006/jmra.1995.9969
39. Parella T, Sánchez-Ferrando F, Virgili A (1997) Improved sensitivity in gradient-based 1D and 2D multiplicity-edited HSQC experiments. J Magn Reson 126:274-277. https://doi.org/10.1006/jmre.1997.1164
40. Rucker SP, Shaka AJ (1989) Broadband homonuclear cross polarization in 2D NMR using DIPSI-2. Mol Phys 68:509-517. https://doi.org/10.1080/00268978900102331
41. Schleucher J, Sattler M, Griesinger C (1993) Coherence selection by gradients without signal attenuation: application to the three-dimensional HNCO experiment. Angew Chem Int Ed 32:1489-1491. https://doi.org/10.1002/anie.199314891
42. Schmidt JM, Ruterjans H (1990) Proton-detected 2D heteronuclear shift correlation via multiple-quantum coherences of the type I_2S. J Am Chem Soc 112:1279-1280. https://doi.org/10.1021/ja00159a077
43. Shaka AJ, Barker PB, Freeman R (1985) Computer-optimized decoupling scheme for wideband applications and low-level operation. J Magn Reson 64:547-552. https://doi.org/10.1016/0022-2364(85)90122-2
44. Shaka AJ, Keeler J, Frenkiel T, Freeman R (1983) An improved sequence for broadband decoupling: WALTZ-16. J Magn Reson 52:335-338. https://doi.org/10.1016/0022-2364(83)90207-X
45. Stelten J, Leibfritz D (1996) Clean HX and H_2X proton selection using gradients: gs H_nX-HYSEL. Magn Reson Chem 34:951-954. https://doi.org/10.1002/(Sici)1097-458x(199611)34:11<951::Aid-Omr3>3.0.Co;2-G
46. Tate S, Masui Y, Inagaki F (1991) Application of the DEPT sequence to the separation of ^{15}NH and $^{15}NH_2$ resonances in ^{1}H-detected ^{15}N single-quantum coherence spectroscopy. J Magn Reson 94:625-630. https://doi.org/10.1016/0022-2364(91)90152-J
47. Tugarinov V, Hwang PM, Ollerenshaw JE, Kay LE (2003) Cross-correlated relaxation enhanced ^{1}H–^{13}C NMR spectroscopy of methyl groups in very high molecular weight proteins and protein complexes. J Am Chem Soc 125:10420-10428. https://doi.org/10.1021/ja030153x
48. Weininger U, Blissing AT, Hennig J, Ahlner A, Liu Z, Vogel HJ, Akke M, Lundström P (2013) Protein conformational exchange measured by ^{1}H $R_{1\rho}$ relaxation dispersion of methyl groups. J Biomol NMR 57:47-55. https://doi.org/10.1007/s10858-013-9764-4

49. Xie T, Saleh T, Rossi P, Kalodimos CG (2020) Conformational states dynamically populated by a kinase determine its function. Science 370:eabc2754. https://doi.org/10.1126/science.abc2754
50. Yamazaki T, Muhandiram R, Kay LE (1994) NMR experiments for the measurement of carbon relaxation properties in highly enriched, uniformly ^{13}C,^{15}N-labeled proteins: Application to $^{13}C^{\alpha}$ carbons. J Am Chem Soc 116:8266-8278. https://doi.org/10.1021/ja00097a037

Figures

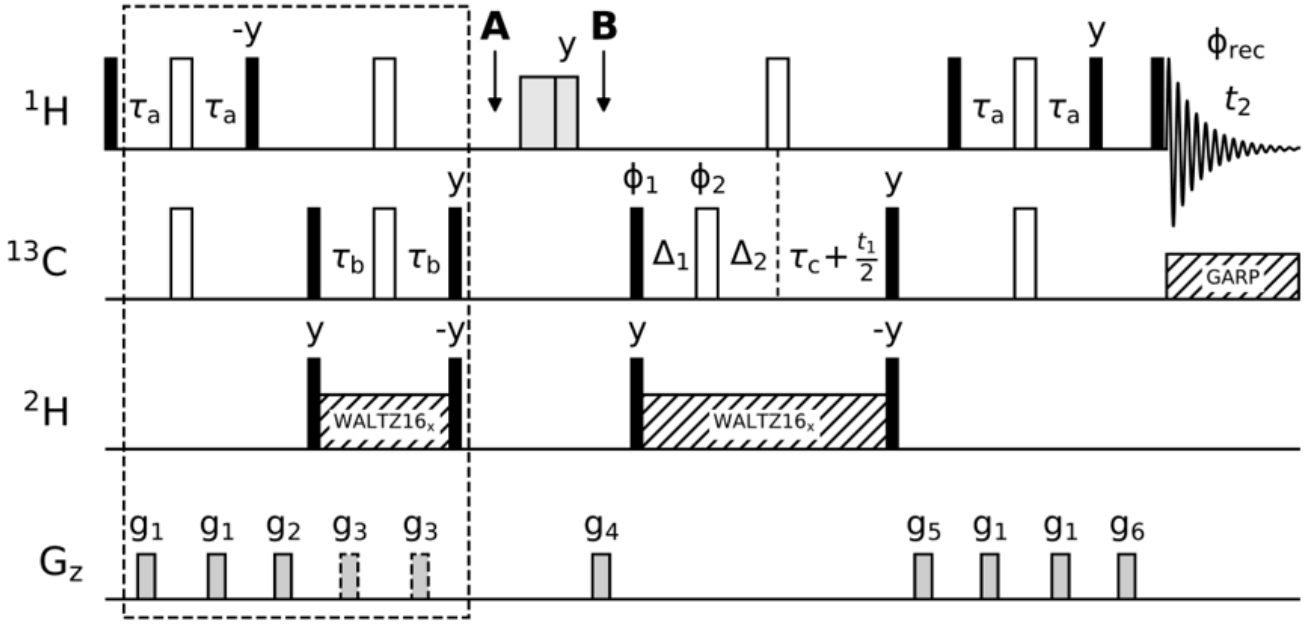


Figure 1

Pulse scheme of CH-selective ^1H–^{13}C HSQC experiment with unenhanced implementation (the ^{13}CH selectivity is active via "-DCH_sel" in ZGOPTNS). 90° (180°) rectangular pulses on ^1H and ^{13}C channels are denoted by *narrow* (*wide*) *bars* and applied at maximum available power, with the exception of ^1H spin-lock purge pulses, which are typically set to ~10 kHz. The forward magnetization transfer from ^1H to ^{13}C can alternatively be performed by replacing refocused INEPT elements in the *dashed rectangle* with DIPSI-2 (Rucker and Shaka 1989) cross-polarization (CP) (via "-Dcp_new" in ZGOPTNS to use any value of CP mixing time τ_{mix}, or "-Dcp_old" to perform integer number of DIPSI-2 cycles. Note that the "-Dcp_new" option may not work on certain old spectrometers). All 180° pulses on ^1H and ^{13}C are applied with G5 shape (Manu and Veglia 2015) to achieve larger bandwidth coverage, and the duration of each G5 pulse is five times of the rectangular 180° pulse at the same power level. The two consecutive ^1H spin-lock purge pulses have durations of 5.0 ms and 3.1 ms (via "-Dmess_flg" in ZGOPTNS) (Messerle et al. 1989). The ^1H carrier is placed on resonance with water (~4.7 ppm) between points "A" and "B", and at the center of ^1H signal region elsewhere. The ^{13}C carrier is placed in the center of ^{13}C signal region.

^{13}C GARP decoupling (Shaka et al. 1985) is applied during free induction decay (FID) acquisition (t_2). The delays used are: $\tau_a = 1/(4^1J_{CH})$, $\tau_c = 1/(4^1J_{CH})$, $\Delta_1 = \max(\tau_c - t_1/2, 0)$, $\Delta_2 = \max(t_1/2 - \tau_c, 0)$ ($\max(a, b)$ indicates the larger value of a and b). The optimal value of τ_b or τ_{mix} is determined with accuracy of 0.01 ms or 0.1 ms based on one-dimensional version of the experiment (Figs. S2, S3). All pulses are applied with phase x unless otherwise indicated. The phase cycles are $\phi_1 = x, -x$; $\phi_2 = x, x, y, y, -x, -x, -y, -y$; $\phi_{rec} = x, -x, -x, x$. The number of transients should be set as multiple of 2. Quadrature detection in the F_1 dimension is achieved by STATES–TPPI of ϕ_1 (Marion et al. 1989). Pulsed field gradients (PFGs) are applied with the following durations (in ms) and strengths (in % maximum): g_1: (0.5, 20%), g_2: (1.0, 65%), g_3: (0.5, 20%), g_4: (1.0, −60%), g_5: (1.0, 60%), g_6: (1.0, 40%). For studying biomolecules with ^{2}H attached to ^{13}C in ^{13}CH groups, ~1 kHz WALTZ-16 (Shaka et al. 1983) ^{2}H decoupling can be applied to achieve better resolution in the F_1 dimension (via "-DD_dec" in ZGOPTNS, with g_3 gradients omitted). The pulse sequence code for Bruker spectrometers is included in the Supplementary Information, and can also be found in the GitHub repository (https://github.com/tyuwen/chsqc_G5).

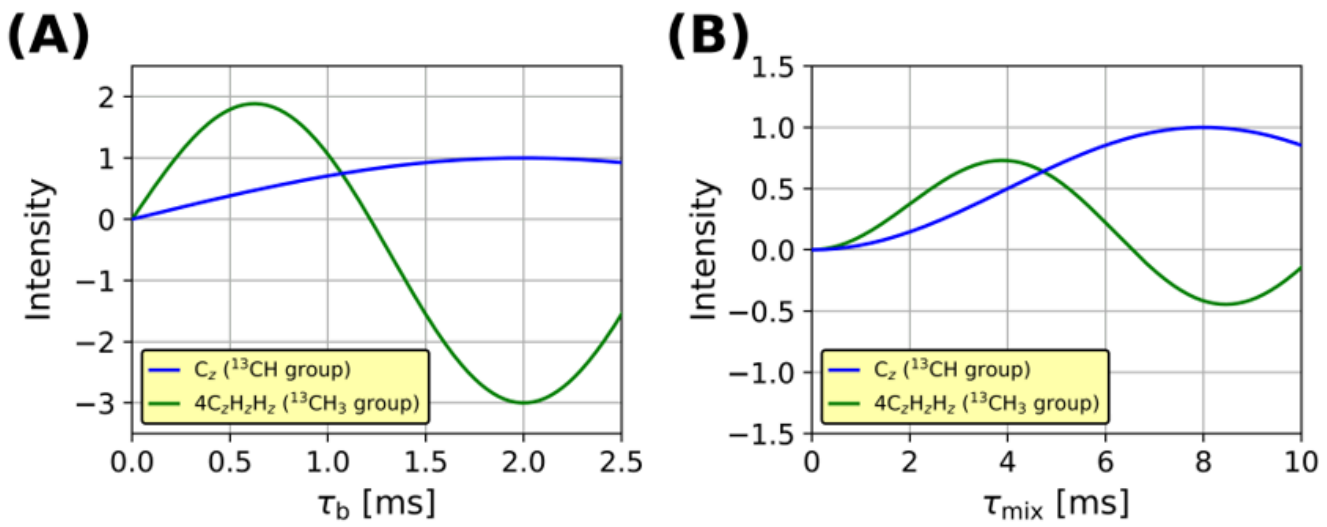


Figure 2

The intensities of different spin orders versus τ_b or τ_{mix} in (A) INEPT-based and (B) CP-based coherence transfer scheme for ^{13}CH and $^{13}CH_3$ groups with the initial density matrix corresponding to spin orders $2C_zH_z$ and H_z, respectively. $^1J_{CH}$ = 125 Hz was used for ^{13}CH and $^{13}CH_3$ moieties in the numerical simulation, and relaxation effects were not included.

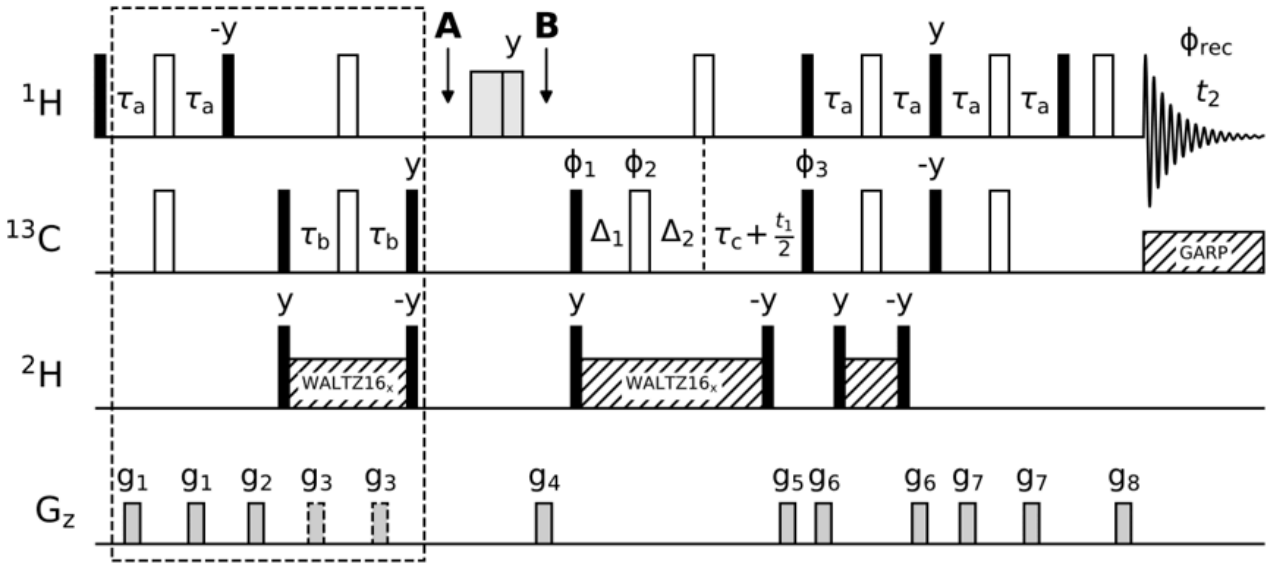


Figure 3

Pulse scheme of CH-selective ^{1}H–^{13}C HSQC experiment with sensitivity-enhanced implementation. Most details are the same as the unenhanced implementation (Fig. 1). The phase cycles are ϕ_1 = *x*, –*x*; ϕ_2 = *x*, *x*, *y*, *y*, –*x*, –*x*, –*y*, –*y*; ϕ_3 = *x*; ϕ_{rec} = *x*, –*x*, –*x*, *x*. The number of transients should be set as multiple of 2. Echo/Anti-Echo selection is achieved by inverting the phase of ϕ_3 together with the sign of gradient g_5 (Kay et al. 1992; Schleucher et al. 1993). Pulsed field gradients (PFGs) are applied with the following durations (in ms) and strengths (in % maximum): g_1: (0.5, 20%), g_2: (1.0, 65%), g_3: (0.5, 20%), g_4: (1.0, –60%), g_5: (0.5, 80%), g_6: (0.5, 50%), g_7: (0.5, 25%), g_8: (0.5, 20.1%). The pulse sequence code for Bruker spectrometers is included in the Supplementary Information, and can also be found in the GitHub repository (https://github.com/tyuwen/chsqc_G5).

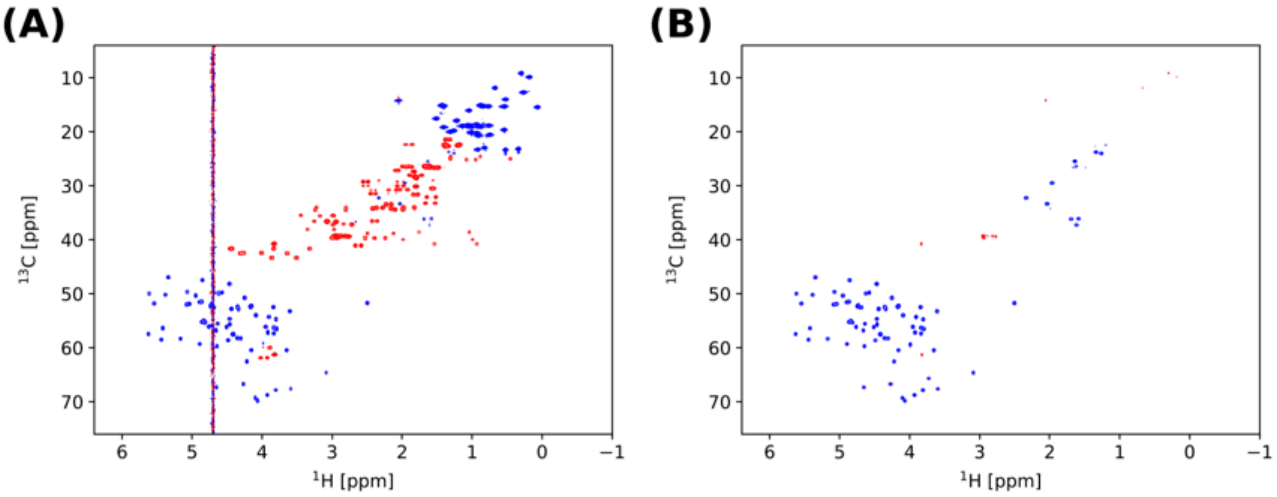


Figure 4

(A) The multiplicity-edited variant of regular $^{1}H–^{13}C$ HSQC and (B) CH-selective $^{1}H–^{13}C$ HSQC (CP-based, sensitivity-enhanced implementation) of [U-^{13}C]-labeled protein L. The *blue* and *red contours* indicate positive and negative peaks, respectively.

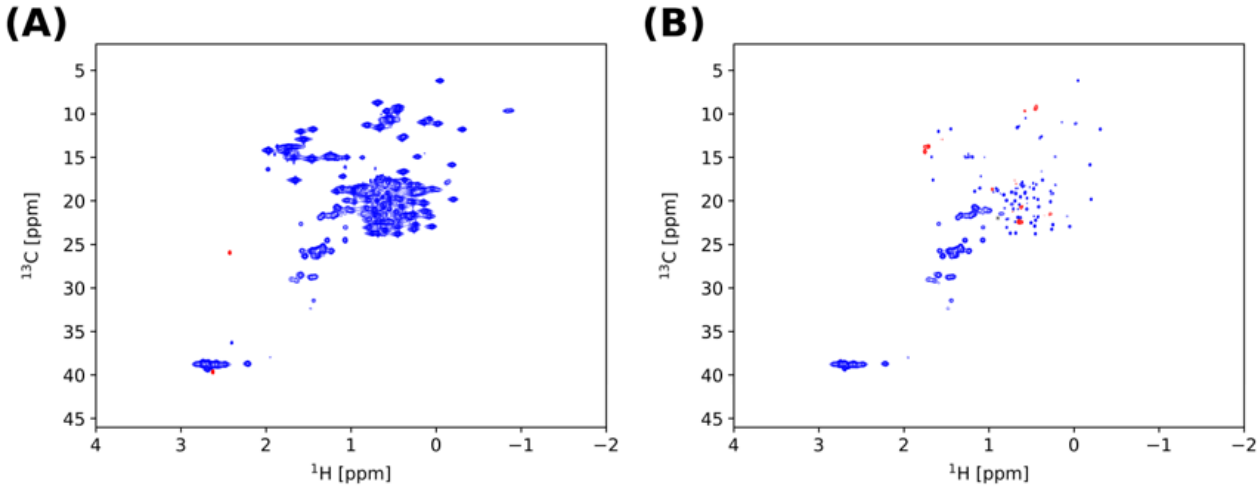


Figure 5

(A) The multiplicity-edited variant of regular $^{1}H–^{13}C$ HSQC and (B) CH-selective $^{1}H–^{13}C$ HSQC (CP-based, unenhanced implementation) of ILVMAT-$^{13}CH_3$ + SAIL-Lys labeled BRAF. The *blue* and *red contours* indicate positive and negative peaks respectively. In Panel B the *"*"* *mark* indicates one ^{13}CH resonance from SAIL-Lys which is overlapped with $^{13}CH_3$ signals in regular $^{1}H–^{13}C$ HSQC (Panel A).

Supplementary Files

This is a list of supplementary files associated with this preprint. Click to download.

- CH3hetcpsupplementaryv2yxty2.pdf
- GraphicAbstract.docx